



Contents lists available at ScienceDirect

International Journal of Applied Earth Observation and Geoinformation

journal homepage: www.elsevier.com/locate/jag

Spatiotemporal dynamics and key climatic influences on vegetation resilience in opencast coal mine dumps after restoration

Hui Wang^a, Chengye Zhang^a, Yaxin Ding^a, Feiyue Li^a, Wanxi Liu^{a,b}, Yan Ma^c, Yingjie Guo^d, Bikram Banerjee^e, Jun Li^{a,*}

^a College of Geoscience and Surveying Engineering, China University of Mining and Technology (Beijing), Beijing 100083, China

^b China Coal Green Energy Technology Co., Ltd., Beijing 100871, China

^c College of Urban and Environmental Sciences, Laboratory for Earth Surface Processes of the Ministry of Education, Peking University, Beijing 100871, China

^d Neimenggu pingzhuang Coal Industry (Group) Co., Ltd., Chifeng City, Inner Mongolia Autonomous Region, Chifeng 024000, China

^e School of Surveying and Built Environment, University of Southern Queensland, Toowoomba, Queensland 4350, Australia

ARTICLE INFO

Keywords:

Mine vegetation resilience
Critical Slowing Down theory
AC(1)
Remote sensing
Opencast coal mine dump

ABSTRACT

Vegetation resilience is crucial for understanding the self-repair and adaptive capacity of regional ecosystems. Opencast coal mine dumps, typical targets for ecological restoration, exhibit highly unstable vegetation ecosystems after restoration, making them prone to state shifts. However, existing studies have limitations in capturing vegetation resilience characteristics and its climatic driving mechanisms. This study addresses these deficiencies by focusing on the Pingzhuang West Opencast Coal Mine dumps, utilizing Critical Slowing Down (CSD) theory and long-term Landsat remote sensing data from 2008 to 2024. We propose 'MultiRes', a pixel-level (30 m) method to calculate vegetation resilience. Unlike traditional fixed-window approaches, MultiRes offers adaptive window sizes with a wide range of stability. We analyzed the spatiotemporal dynamics of vegetation resilience after restoration, evaluated the effectiveness of vegetation restoration, and quantitatively assessed the impact of key climatic drivers across different phases. Results reveal that: (1) After restoration, vegetation resilience at each dump experienced three phases: initial enhancement, decline, and renewed enhancement. (2) Vegetation resilience improved significantly compared to the initial fragile ecosystem, with over 88 % of the area showing improvement, especially at Taipingdi, where the enhancement rate reached 99.85 %. (3) The influence of key climatic drivers remained consistent within each dump across all phases, particularly in the first and third phases. Areas dominated by a single climatic driver generally showed more significant changes than those influenced by combined drivers. These findings demonstrate that vegetation resilience captures stage-specific ecological patterns that NDVI alone cannot detect, thereby supporting adaptive restoration and climate-informed management in mining environments.

1. Introduction

Vegetation is a vital component of ecosystems and a sensitive indicator of climate change, essential for maintaining regional and global ecosystem stability (Seddon et al., 2016). Increasingly, studies have emphasized the role of vegetation beyond natural landscapes, particularly trees, grasses, and urban green infrastructures, in mitigating environmental risks, regulating hydrology, and enhancing climate resilience in urban environments (e.g., Ghalehtemouri et al., 2024(a); Ghalehtemouri et al., 2024(b); Golestani et al., 2024; Kamran et al., 2024; Nasr et al., 2025). However, mine rehabilitation significantly

alters topography and landscape structure, impacting local vegetation cover and ecological function (Antwi et al., 2008; Worlanyo and Jiangfeng, 2021). Opencast coal mine dumps, often targeted for ecological restoration, are typically characterized by rocky, nutrient-deficient substrates prone to frequent erosion. These conditions result in fragile vegetation struggling to achieve stability after restoration (Hancock et al., 2020; Wang et al., 2020; Li et al., 2024(b)). Therefore, monitoring vegetation's self-repair and adaptive capacity in such environments is crucial.

The capacity of vegetation ecosystems for self-repair and adaptation largely depends on their resilience—the ability to withstand and recover

* Corresponding author at: No.11 Xueyuan Road Street, Haidian District, Beijing, China.

E-mail address: junli@cumtb.edu.cn (J. Li).

<https://doi.org/10.1016/j.jag.2025.104646>

Received 6 February 2025; Received in revised form 6 May 2025; Accepted 31 May 2025

Available online 4 June 2025

1569-8432/© 2025 The Authors. Published by Elsevier B.V. This is an open access article under the CC BY-NC-ND license (<http://creativecommons.org/licenses/by-nc-nd/4.0/>).

from environmental disturbances (Scheffer et al., 2009; Van Meerbeek et al., 2021). Low vegetation resilience increases sensitivity to disturbances and the risk of sudden, permanent ecological degradation (Scheffer et al., 2015; Dakos et al., 2015). McDougall et al. (2013) provided long-term empirical evidence from a degraded grassland system in western North America to support these views. Despite extensive research on climate change, the response of vegetation resilience to climatic drivers in mining areas remains insufficiently explored (Liu et al., 2024). Monitoring the spatiotemporal dynamics of vegetation resilience and analyzing key climatic drivers in mining dumps are essential for assessing vegetation's self-repair and adaptive capacity and understanding climate-driven mechanisms, informing targeted approaches to vegetation restoration.

Traditional studies on vegetation dynamics in mining areas have primarily used vegetation indices to monitor changes in vegetation cover (e.g., Li et al., 2015; Zhang et al., 2019; Hutayanon and Somprasong, 2023). This method, facilitated by remote sensing technology, allows for efficient and broad-scale monitoring of vegetation health. Li et al. (2015) compared Normalized Difference Vegetation Index (NDVI), Normalized Burn Ratio (NBR), and Normalized Difference Moisture Index (NDMI) and found that NDVI effectively distinguishes green vegetation. Zhang et al. (2019) and Zhang et al. (2023) utilized remote sensing imagery to compute fractional vegetation coverage (FVC) and other indices, reconstructing the recovery process of coal mine dumps. In Southeast Asia, Hutayanon and Somprasong (2023) applied spatial-integrated analysis with NDVI to monitor vegetation growth in the Mae Moh coal mine area. However, while vegetation indices, particularly NDVI, effectively reflect average level of greening status, they have limitations in characterizing vegetation's self-repair and adaptive capacity in response to environmental disturbances. Understanding ecological adaptability, especially after restoration, requires more sensitive metrics like vegetation resilience (Boulton et al., 2022).

CSD theory offers a practical framework for characterizing vegetation resilience, positing that resilience declines as an ecosystem nears a collapse threshold, evidenced by a slowing recovery rate (Wichers et al., 2016). This approach has been effectively applied to assess vegetation resilience under various environmental disturbances, including climate change, natural disasters, and human activities. For example, Flores et al. (2024) predict that up to 47% of the Amazon rainforest's vegetation resilience may decline by 2050, driven by unprecedented stress from warming temperatures, extreme droughts, deforestation and fires. Similarly, Van Belzen et al. (2017) applied CSD theory to explore vegetation resilience in tidal zones across Europe and North America. Concurrently, Wang et al. (2023)(b) investigated how vegetation greening correlates with resilience in China's Loess Plateau. These studies underscore CSD's broad applicability across diverse ecosystems, offering valuable theoretical insights and fresh perspectives on evaluating vegetation resilience in opencast coal mine dumps.

To address deficiencies in the dynamic monitoring, as well as quantification of vegetation self-repair and adaptive capacity in opencast coal mine dumps, this study applies Critical Slowing Down (CSD) theory to this specific scenario. We further investigate the effects of climatic drivers on vegetation resilience after restoration. We selected a typical study area in China, the Pingzhuang West Opencast Coal Mine dumps. This study aims to (1) Propose a method for developing an indicator of vegetation self-repair and adaptive capacity using an adaptive window decomposition, (2) explore the temporal and spatial characteristics of vegetation resilience, (3) evaluate changes in vegetation resilience across different phases after restoration quantitatively, and (4) quantify the impact of key climatic drivers at different phases of the recovery process. The findings provide a reliable basis for evaluating vegetation resilience, identifying and predicting critical stages of recovery, and enhancing the understanding of climatic influences on vegetation restoration, ultimately supporting the development of effective ecological restoration strategies.

2. Study area and data

2.1. Study area overview

The Pingzhuang West Opencast Coal Mine is an ecologically vulnerable region, where the surrounding environment is severely degraded due to the idleness of the pit after resource extraction, and it faces severe climatic conditions such as high winds, droughts, and cold, recognized as a critical area for ecosystem conservation and restoration in China. The mine is in Yuanbaoshan District, Chifeng City, Inner Mongolia Autonomous Region (Fig. 1). The study area experiences a mid-temperate, semi-arid continental climate characterized by cold, dry winters and short, humid summers, with most precipitation occurring during the summer. The vegetation in the region is primarily grassland. The mine encompasses three external rehabilitated areas: Taipingdi dump, Shanhou dump, and Sanjia dump, which cover approximately 526.42 ha, 64.88 ha, and 552.81 ha, respectively. The research period of this study follows the implementation of vegetation restoration measures. Specifically, restoration efforts began in 2008 at the Taipingdi and Shanhou dumps, and in 2014 at Sanjia dump. Subsequent to these efforts, the dumps have experienced several years of natural regrowth.

2.2. Data sources and preprocessing

The study utilizes remotely sensed data comprising Landsat satellite images and high-resolution imagery. Landsat satellite images acquired between December 2005 and February 2024 were processed on the Google Earth Engine (GEE) platform, with the Auto-NDVI_{cb} algorithm developed by our team (Li et al., 2024(a)) applied to automatically generate seasonal maximum NDVI data. The algorithm consists of four main steps: (1) calculation of time-series NDVI images, (2) automatic selection of the reference NDVI image, (3) construction of the calibration model, and (4) batch calibration and fusion. The GEE script is available in the *Code Availability section*. This processing incorporated surface reflectance (SR) datasets from the Landsat 5 Thematic Mapper (TM), Landsat 7 Enhanced Thematic Mapper Plus (ETM+) and Landsat 8 Operational Land Imager (OLI). High-resolution imagery from the Gaofen-1 satellite was sourced from the Land Observation Satellite Data Service Platform of the China Centre for Resources Satellite Data and Application (<https://data.cresda.cn/>). High-resolution imagery of the study area from 2024 was imported into ArcGIS, and the vector boundaries of the three dumps and slope were manually delineated.

Daily meteorological data, including temperature, precipitation, and net solar radiation from 2008 to 2024, were sourced from the ERA5-Land reanalysis dataset (<https://www.ecmwf.int>) (Muñoz Sabater, 2021). Furthermore, our team installed the BX-H1100 multifunctional meteorological station within the study area to collect hourly observations from January to June 2024. The collected field data were used to calibrate the ERA5-Land temperature data using a simple linear regression model. Detailed information on the field data collection and calibration are provided in Supplementary Materials A1.

3. Methods

3.1. Vegetation resilience calculation

Fig. 2 illustrates the workflow of the MultiRes Method, a pixel-adaptive approach developed to calculate vegetation resilience by optimizing the decomposition of seasonal NDVI time series. Specifically, MultiRes identifies the optimal sliding window size for each pixel during Seasonal and Trend decomposition using Loess (STL), thereby ensuring that the stability of the resulting residuals is not affected by the choice of window size. Seasonal maximum NDVI was used as the input to generate seasonal vegetation resilience maps at a spatial resolution of 30 m, suitable for localized analyses such as dumps.

Initially, the Auto-NDVI_{cb} algorithm was applied to automatically

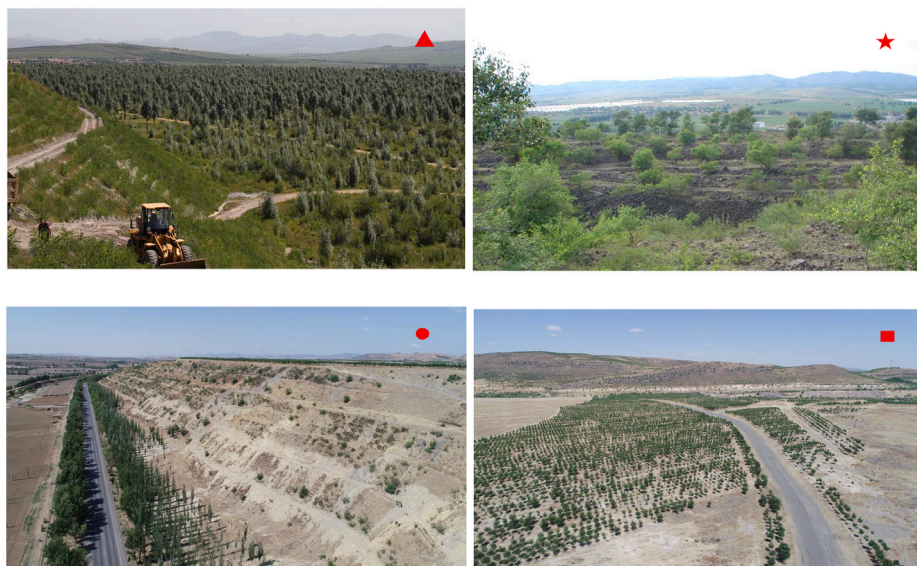
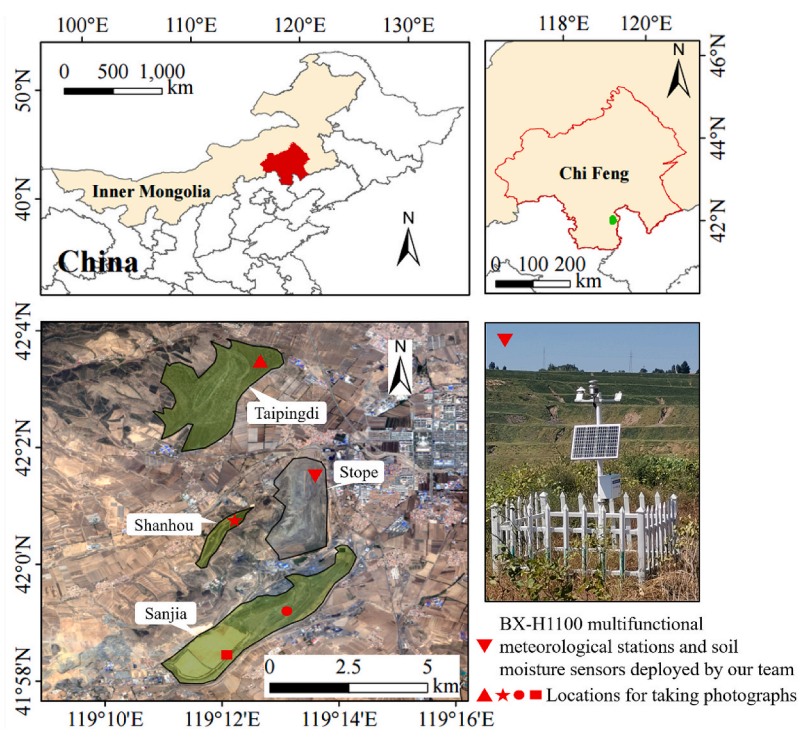


Fig. 1. Geographical location of Pingzhuang West Opencast Coal Mine. Photographs taken in August 2024.

generate seasonal maximum NDVI data from December 2005 to February 2024. This algorithm selects the NDVI image with the highest mean value within the research period as the reference image. Based on the consistency of tones between similar geographical entities, mathematically represented by the similarity of cumulative distribution functions, it establishes a mapping relationship of NDVI pixel values between all NDVI images and the reference image. This effectively addresses the issues of abnormal mosaic lines and value biases caused by temporal inconsistencies in traditional NDVI products. Furthermore, a cross-sensor calibration model is established to solve the inconsistency of NDVI values caused by different sensors. Details of this calibration can be found in Supplementary Material A2. The NDVI formula is presented in Equation (1).

$$NDVI = \frac{\rho_{NIR} - \rho_R}{\rho_{NIR} + \rho_R} \quad (1)$$

where ρ_{NIR} is the surface reflectance in the near-infrared band, and ρ_R is the surface reflectance in the red band. NDVI is widely used to quantify vegetation greenness, as healthy vegetation strongly reflects near-infrared light and absorbs red light (Huang et al., 2021).

Subsequently, we employed the Multi-Window-Finder (MWF) method to determine the optimal sliding window size for STL decomposition of the seasonal maximum NDVI data (Imani and Keogh, 2021). This method evaluates a range of candidate window sizes and selects the one that minimizes the moving average error. The applicability and accuracy of MWF have been verified using 250 time-series datasets from diverse domains in the Knowledge Discovery and Data Mining (KDD) Cup. We applied this method across the study area to generate the optimal window size for each pixel, as shown in Fig. 3.

Next, the pixel-level optimal window sizes derived from the MWF method (Fig. 3) were used as inputs for STL. STL separates each NDVI

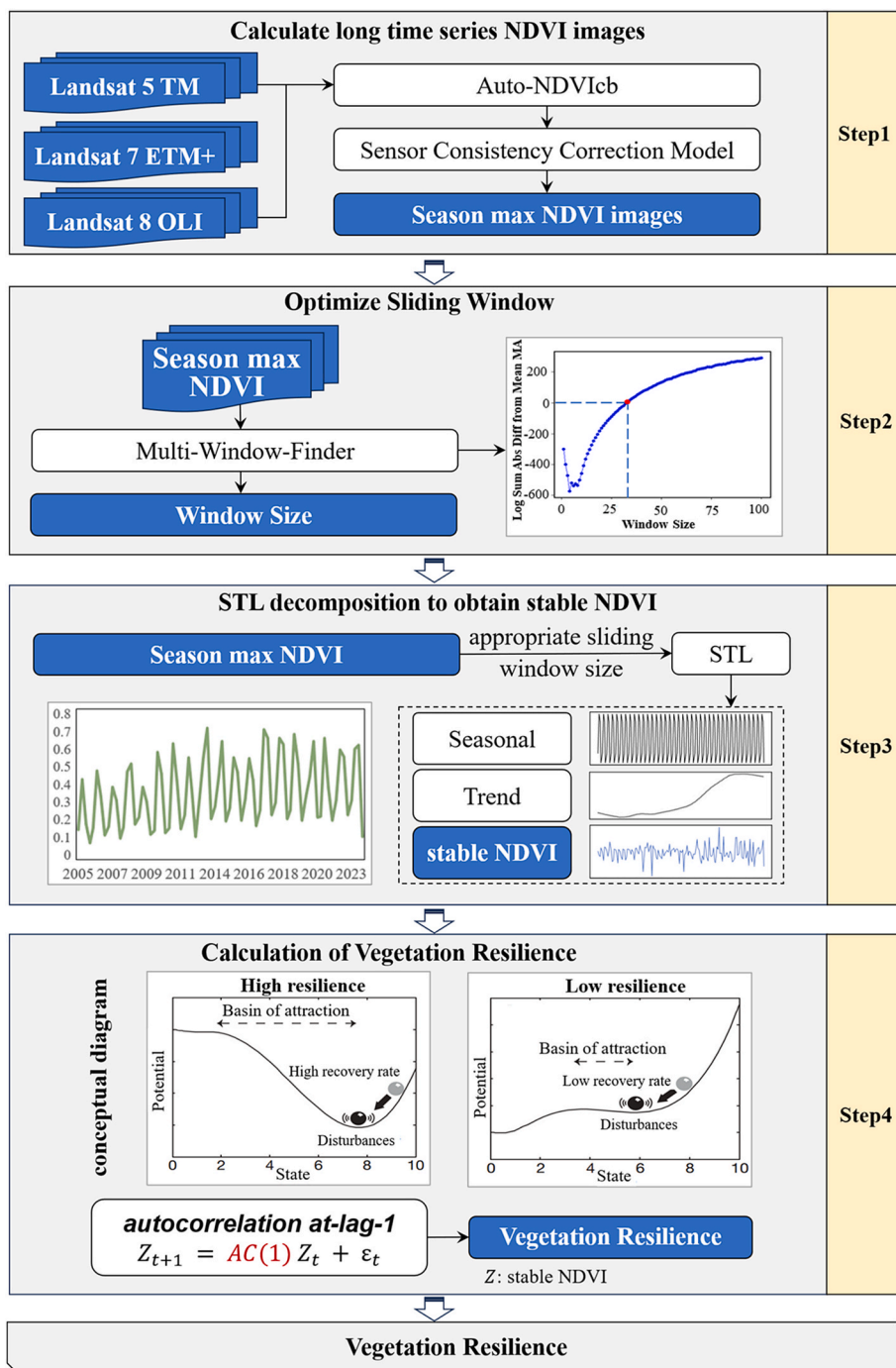


Fig. 2. Workflow of the MultiRes Method.

time series into trend, seasonal, and residual components through locally weighted regression (Wang et al., 2012). By incorporating the spatially adaptive window sizes into the decomposition process, we effectively removed long-term trends and seasonal effects, resulting in more stable NDVI residuals suitable for subsequent resilience analysis based on CSD theory (Apaydin et al., 2021).

To evaluate the stability of NDVI residual components obtained through STL decomposition, we utilized classical methods, including Augmented Dickey-Fuller (ADF), Kwiatkowski-Phillips-Schmidt-Shin (KPSS) test and variance measures, to explore the suitability and robustness of the MultiRes. The ADF test is based on the null hypothesis that the time series is non-stationary, whereas the KPSS test assumes stationarity (Van Greunen et al., 2014). As shown in Table 1, in the

traditional fixed-window approach, the ADF p-values and variance exhibited substantial fluctuations across different window sizes, particularly when the window size was 50 at the Shanhou dump and 40 or 50 at the Sanjia dump. In these cases, the residual series even failed to meet the requirements for subsequent vegetation resilience analysis. This indicates that the traditional method has significant window sensitivity defects and its stability is difficult to guarantee. By contrast, the MultiRes adaptively determines the optimal window for each pixel, maintaining stable residuals across diverse regions and environmental conditions.

Finally, according to CSD theory, the ecosystem becomes increasingly susceptible to state shifts as vegetation resilience diminishes, leading to slower recovery after disturbances (Dakos et al., 2012; Meisel

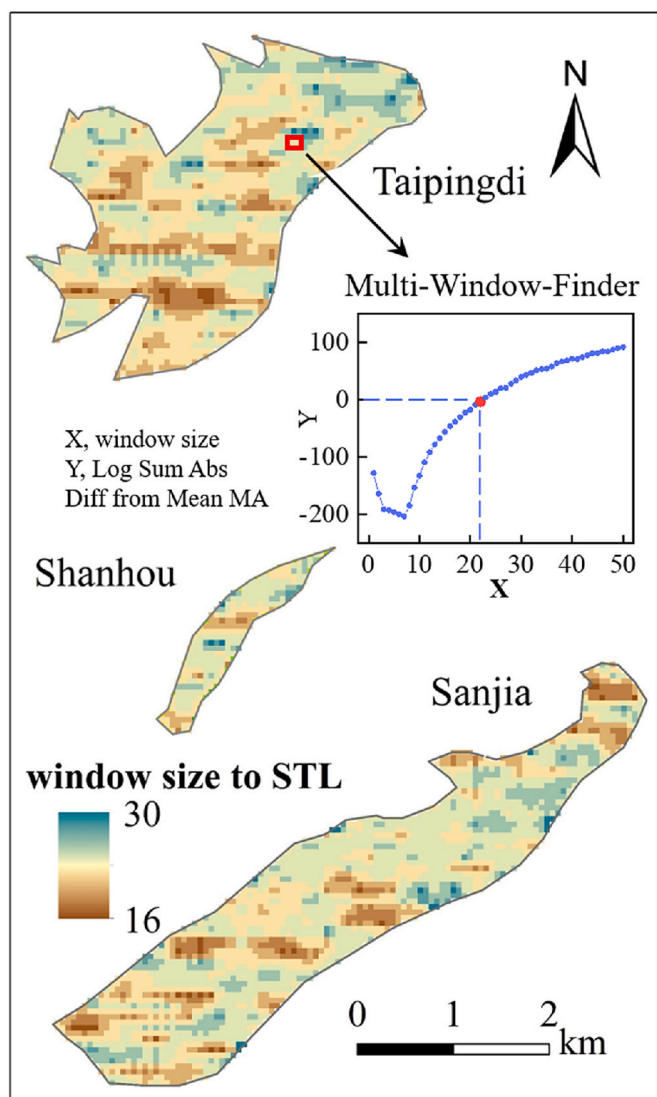


Fig. 3. Pixel-level optimal window sizes for STL decomposition.

et al., 2015; Diks et al., 2019). Under these conditions, the similarity between successive time points in the dataset increases, leading to heightened temporal autocorrelation in the vegetation index (Scheffer et al., 2009). Consequently, this study employs the first-order autocorrelation coefficient, AC(1), as an indicator of vegetation resilience, detailed in Equation (2). AC(1) values range from -1 to 1, where higher values signify reduced resilience and a heightened risk of succumbing to disturbances (Dakos et al., 2010; Scheffer et al., 2015). For instance, Smith and Boers (2022) demonstrated that increasing AC(1) values revealed persistent losses of vegetation resilience from 1992 to 2017 in high-latitude regions, southern Africa, and parts of Australia.

Table 1

Comparison of STL decomposition residuals between the MultiRes method and traditional fixed-window approaches.

Window size	Taipingdi ADF p-value	KPSS p-value	Variance	Shanhou ADF p-value	KPSS p-value	Variance	Sanjia ADF p-value	KPSS p-value	Variance
10	0.0103	0.1000	0.0043	0.0121	0.1000	0.0034	0.0138	0.1000	0.0047
20	0.0101	0.1000	0.0040	0.0105	0.1000	0.0031	0.0111	0.1000	0.0043
30	0.0105	0.1000	0.0045	0.0280	0.1000	0.0039	0.0253	0.1000	0.0050
40	0.0124	0.1000	0.0046	0.0474	0.1000	0.0042	0.0564	0.0999	0.0050
50	0.0142	0.0999	0.0047	0.0599	0.1000	0.0044	0.0985	0.0983	0.0056
MultiRes	0.0100	0.1000	0.0038	0.0101	0.1000	0.0028	0.0102	0.1000	0.0039

$$Z_{t+1} = AC(1)Z_t + \epsilon_t \tag{2}$$

where Z_t is the stable seasonal maximum NDVI time series value at time t , Z_{t+1} is the stable seasonal maximum NDVI time series value at time $t + 1$, and ϵ_t is the residual obtained using ordinary least squares.

We utilized an equal-interval classification method for NDVI levels (Hu and Xia, 2019), vegetation resilience is categorized into five levels based on AC(1) values, as depicted in Table 2.

3.2. Temporal trend analysis

To investigate the changes in vegetation resilience after restoration, Kendall's τ was used to assess the trends in the AC(1) values. Kendall's τ is a non-parametric method that measures the correlation between two variables by comparing the rank order of paired data points (Shiekh and El-Hashash, 2022). A key advantage of this approach is its independence from standard distribution assumptions and its robustness in handling outliers (Xu et al., 2013), making it particularly suited for environmental and meteorological studies. The formula for Kendall's τ is detailed in Equation (3) – (6) (Kendall, 1938).

$$\tau(X, Y) = \frac{N_c - N_d}{\sqrt{N_0 - T_X} \sqrt{N_0 - T_Y}} \tag{3}$$

where

$$N_0 = N(N - 1)/2 \tag{4}$$

$$T_X = \sum_{p=1}^P t_p(t_p - 1)/2 \tag{5}$$

$$T_Y = \sum_{q=1}^Q u_q(u_q - 1)/2 \tag{6}$$

where N_0 is the total number of discordant pairs, while T_X and T_Y are the number of ties in datasets X and Y , respectively. t_p and u_q are the lengths of the ties in the p^{th} and q^{th} ranks in datasets X and Y , P and Q are the numbers of tied groups in datasets X and Y . This study's datasets X and Y correspond to the time series and AC(1) values. Each pixel's AC(1) value is treated as a time series, and Kendall's τ is calculated to evaluate the AC(1) trend over each period. The value of τ ranges from [-1, 1], where $\tau = 1$ indicates a perfect positive correlation (i.e., consistent trend), $\tau = -1$ indicates a perfect negative correlation (i.e., opposing trend), and τ close to 0 suggests no significant correlation in the trend of AC(1) over time.

Table 2

Classification criteria for vegetation resilience levels based on AC(1).

AC(1) range	vegetation resilience level
$AC(1) \geq 0.6$	very low vegetation resilience
$0.6 > AC(1) \geq 0.2$	low vegetation resilience
$0.2 > AC(1) \geq -0.2$	medium vegetation resilience
$-0.2 > AC(1) \geq -0.6$	high vegetation resilience
$AC(1) < -0.6$	very high vegetation resilience

3.3. Vegetation resilience effectiveness evaluation

The effectiveness of vegetation resilience enhancement or reduction was quantified by calculating the difference in resilience between the current state and the initial state when restoration measures were implemented. The calculation method is provided in Equation (7).

$$D_value = AC(1)_n - AC(1)_i \tag{7}$$

where D_value is the change in vegetation resilience at the dump over a given period. AC(1)_n and AC(1)_i represent the AC(1) values at the end and beginning of the study period, respectively. A D_value less than 0 indicates an enhancement in vegetation resilience, while a positive D_value signifies a decline in vegetation resilience.

3.4. Contribution analysis of key climatic influences

The Lindeman, Merenda, and Gold (LMG) model was used to allocate the relative contributions of each independent variable in the regression model (Grömping, 2007), distinguishing the contributions of key climatic drivers (average temperature, total precipitation, and average net solar radiation) to vegetation resilience. R² represents the proportion of the variability in the dependent variable that the model explains. The LMG method decomposes R² by considering the order of regression variables, averaging the unweighted R² for each variable sequence, thus effectively avoiding the effects of variable order. Ultimately, the total R² is decomposed into non-negative components for each regression variable (Yao et al., 2018). Compared to other decomposition methods, the LMG method effectively avoids the effects of regression variable order, thereby providing an accurate measure of the relative importance of each factor. It has been widely applied in meteorological research (Li et al., 2021; Yang et al., 2022; Wang et al., 2023(a)). In this study, we implemented the method using the 'Relaimpo' package in R software.

Based on analyzing the contributions of the three key climatic drivers to vegetation resilience, this study defined and classified the dominant climatic drivers for each pixel, as shown in Table 3. C_P, C_T, and C_R represent the contributions of precipitation, temperature, and net solar radiation to vegetation resilience.

4. Results

4.1. Spatiotemporal dynamics and trends of vegetation resilience in the dumps after restoration

The spatiotemporal dynamics and trends of vegetation resilience in the dumps after restoration were observed by analyzing the AC(1) time series. Taipingdi and Shanhou began vegetation restoration measures in 2008, while Sanjia started in 2014. At this time, the dumps experienced significant anthropogenic disturbances. Fig. 4 presents the seasonal

Table 3
Definition and classification criteria of dominant climatic drivers influencing vegetation resilience.

Dominant Drivers	Criteria	Description
PRCP	C _P ≥ 1/3 & C _T < 1/3 & C _R < 1/3	Dominated by Precipitation
TEMP	C _T ≥ 1/3 & C _P < 1/3 & C _R < 1/3	Dominated by Temperature
NSSR	C _R ≥ 1/3 & C _P < 1/3 & C _T < 1/3	Dominated by Net Solar Radiation
PRCP & TEMP	C _P ≥ 1/3 & C _T ≥ 1/3 & C _R < 1/3	Dominated by Precipitation and Temperature
PRCP & NSSR	C _P ≥ 1/3 & C _R ≥ 1/3 & C _T < 1/3	Dominated by Precipitation and Net Solar Radiation
TEMP & NSSR	C _T ≥ 1/3 & C _R ≥ 1/3 & C _P < 1/3	Dominated by Temperature and Net Solar Radiation

average NDVI and AC(1) time series of the dumps after restoration. Fig. 5 illustrates the spatial distribution of vegetation resilience trends across different phases. Figs. 4 and 5 indicate that vegetation resilience experienced three distinct phases at the dumps: significant enhancement, decline, and renewed enhancement. Currently, Taipingdi and Shanhou are in the third phase, while Sanjia, which started restoration later, is transitioning between the second and third phases. Fig. 6 depicts the spatial distribution of annual maximum vegetation resilience from 2008 to 2021 in the study area, and Fig. 7 shows the classification results of annual maximum vegetation resilience in the dumps after restoration. Figs. 6 and 7 indicate that the year of restoration was marked by the lowest vegetation resilience, predominantly classified as “low” and “medium,” indicating that the self-repair and adaptive capacity of the vegetation ecosystem were severely threatened.

First Phase: Significant Enhancement of Vegetation Resilience.

During the first phase, vegetation resilience significantly improved following the implementation of restoration measures, enhancing the ecosystem’s self-repair and adaptive capacity. Among the dumps, Sanjia exhibited the fastest improvement in vegetation resilience, with Kendall’s τ of −0.884, followed by Shanhou and Taipingdi. Fig. 5 (b) indicates that most areas within the three dumps exhibited increased vegetation resilience during this phase. By the end of the first phase, the dominant type of annual maximum vegetation resilience at Taipingdi (in 2012) was classified as “high.” However, frequent vehicle and machinery movement caused soil compaction and surface erosion, resulting in “medium” and “low” vegetation resilience on north–south dirt road through Taipingdi, with no significant improvement. Similarly, Shanhou (in 2015) showed predominantly “high” vegetation resilience, with two dirt roads traversing the western and central portions of the dump classified as “medium.” Sanjia (in 2019) had a mix of “high” and “medium” vegetation resilience.

Second Phase: Decline in Vegetation Resilience.

In the second phase, vegetation resilience declined, indicating a reduction in the ecosystem’s self-repair and adaptive capacity. Taipingdi experienced the most rapid decline, followed by Sanjia and Shanhou. Fig. 5 (c) shows that most areas in Taipingdi and Shanhou experienced decrease vegetation resilience, particularly in the central Taipingdi and northern Shanhou. Sanjia also showed a general decline in vegetation resilience, with sporadic areas of improvement in the northern and central regions. By the end of the second phase, the annual maximum vegetation resilience of both Taipingdi and Shanhou (in 2017) was mainly classified as “medium.” At Sanjia (in 2021), the vegetation resilience was predominantly “high” and “medium,” with a dispersed spatial distribution.

Third Phase: Renewed Enhancement of Vegetation Resilience.

In the third phase, vegetation resilience improved once more, indicating enhanced self-repair and adaptive capacity of the ecosystem. Taipingdi showed a faster rate of improvement, with Kendall’s τ of −0.723, while Shanhou exhibited a slower recovery, with Kendall’s τ of −0.532. As shown in Fig. 5 (d), most areas in Taipingdi exhibited an increasing trend in vegetation resilience, with the majority of the annual maximum resilience levels classified as “high” and isolated patches in the northern part classified as “very high.” The dirt road in the southern and central parts continued to be classified as “medium.” At Shanhou, the two dirt roads did not show a clear trend of improvement, with the vegetation resilience levels remaining mixed, primarily classified as “high” and “medium,” with some areas along the western side and the roads showing “low” vegetation resilience.

4.2. Evaluating vegetation resilience across different phases

This section quantitatively evaluates changes in vegetation resilience throughout the study period and across each phase (Phase 1, Phase 2, and Phase 3), labeled as D_value, D1_value, D2_value, and D3_value, as shown in Fig. 8 (e), (f), (g), and (h). Fig. 8 (a) illustrates the initial spatial distribution of vegetation resilience when restoration began, while Fig. 8

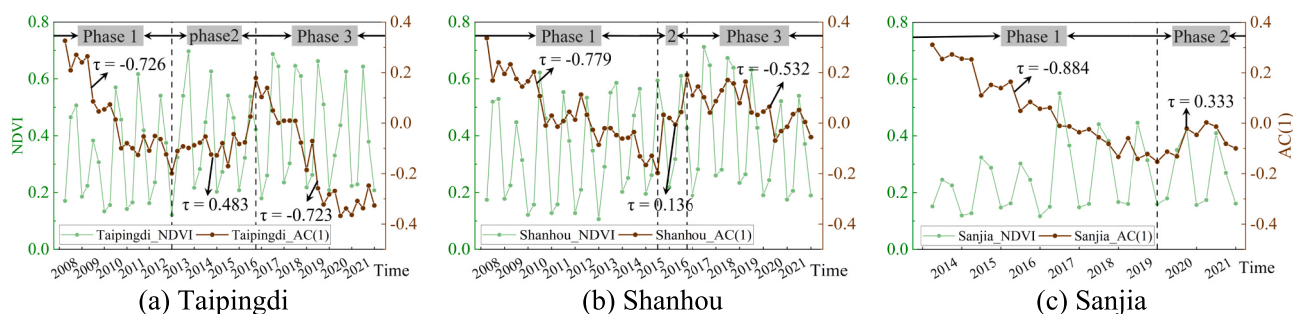


Fig. 4. Seasonal average NDVI and AC(1) time series for each dump after restoration.

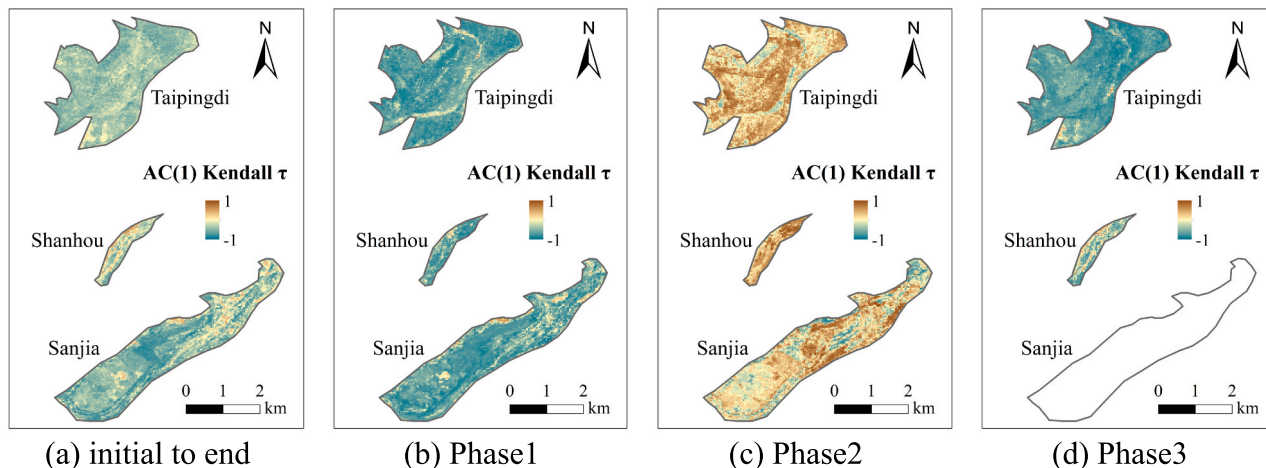


Fig. 5. Spatial distribution of vegetation resilience trends across different phases in the dumps.

(b), (c), and (d) illustrate the spatial distribution of vegetation resilience at the end of Phases 1, 2, and 3, respectively. Table 4 summarizes the proportions of areas where vegetation resilience either enhanced or declined.

Overall, vegetation resilience at the dumps improved significantly from the initial fragile ecosystem, showing a gradual increase in self-repair and adaptive capacity. Among the three dumps, more than 88 % of the area experienced enhancements in vegetation resilience. Field surveys indicated that areas with favorable soil conditions and loose soil texture showed more pronounced increases in vegetation resilience. For instance, Taipingdi enhanced 99.85 % of its area, most notably on the eastern and western sides. Conversely, areas with hard soil or residual coal slag showed limited vegetation resilience improvement, with some areas even exhibiting a decline, particularly near dirt roads subjected to vehicle compaction. Sanjia showed a resilience improvement in 94.04 % of its area. However, the northeast side, which contained residual coal slag, experienced a decline in vegetation resilience, hindering vegetation growth. Shanhou exhibited an increase in vegetation resilience in 88.58 % of its area, while vegetation resilience decreased near the two dirt roads in the western and central regions. These findings indicate that soil physical properties, particularly looseness and disturbance levels, are key to vegetation resilience.

During the first phase, vegetation resilience generally improved across all dumps, with enhancements in over 95 % of each are. Specifically, at Taipingdi, 98.65 % of the area experienced improvement, while declines were mainly concentrated around the central dirt road. At Shanhou, vegetation resilience increased in 99.69 % of the area. Sanjia saw enhancement in 95.02 % of its area, with declines predominantly occurring in the southwest mounds and the northeast side. In the second phase, there was a widespread decline in vegetation resilience across the dumps, particularly in Taipingdi and Shanhou, where declines affected

97.17 % and 99.38 % of the areas, respectively. At Sanjia, 55.73 % of the area showed a decline, primarily in the southwest reclamation area that had been leveled and in the central region. In the third phase, 99.26 % of Taipingdi and 83.74 % of Shanhou showed increased vegetation resilience, albeit at a lower degree than in the first phase.

4.3. Influence of key climate drivers on vegetation resilience

This section explores the impacts of three key climate drivers, total precipitation (TotalPrecip), mean temperature (meanTemp), and mean net solar radiation (meanSolar) on vegetation resilience. Fig. 9 presents the median contributions of key climate drivers to vegetation resilience in each phase at the dumps. We observed a significant pattern: the ranking of climatic drivers remained consistent within each dump throughout the phases, even though it differed across the dumps. This indicates that, although climatic conditions fluctuated, the interaction patterns and weighting among the three drivers did not change significantly. Fig. 10's ternary diagrams illustrate the contributions from combinations of these drivers, where each point represents a pixel's contribution, and the point density indicates the frequency of these combinations within the dumps. The similar shapes of the ternary diagrams in the first and third phases suggest stable vegetation resilience during both the enhancement and renew enhancement phases. In contrast, the distinct shape in the second phase, characterized by a decline in vegetation resilience, indicated a shift in the influence of climatic drivers. Based on the classification of dominant climatic drivers in Table 3, Fig. 11 and Table 5 depict the spatial distribution and proportions of areas influenced by six types of dominant climatic drivers after restoration. Areas dominated by a single climatic driver generally covered more of the dump than those influenced by combined drivers, with precipitation and net solar radiation playing key roles in vegetation

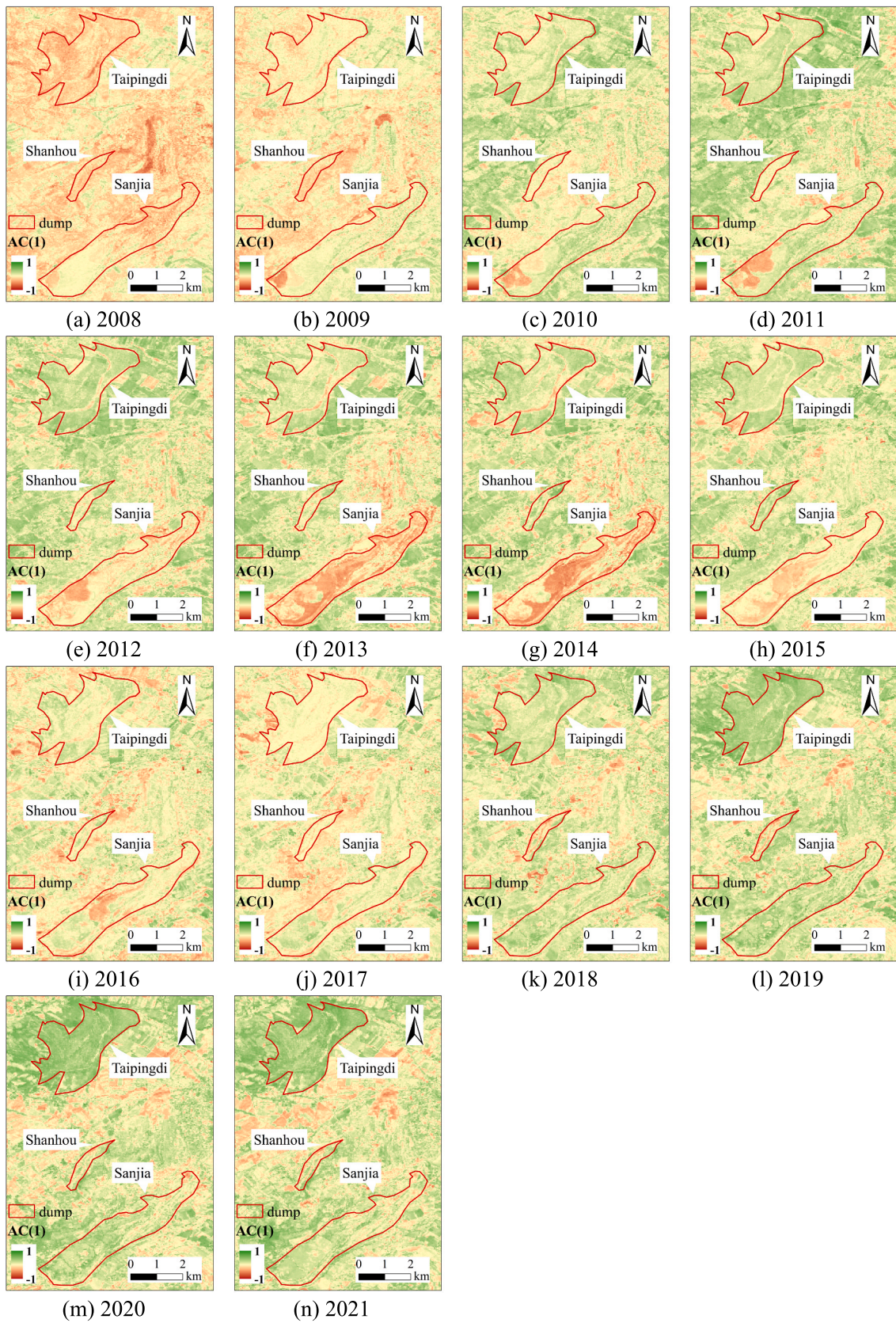


Fig. 6. Spatial distribution of annual maximum vegetation resilience in the study area.

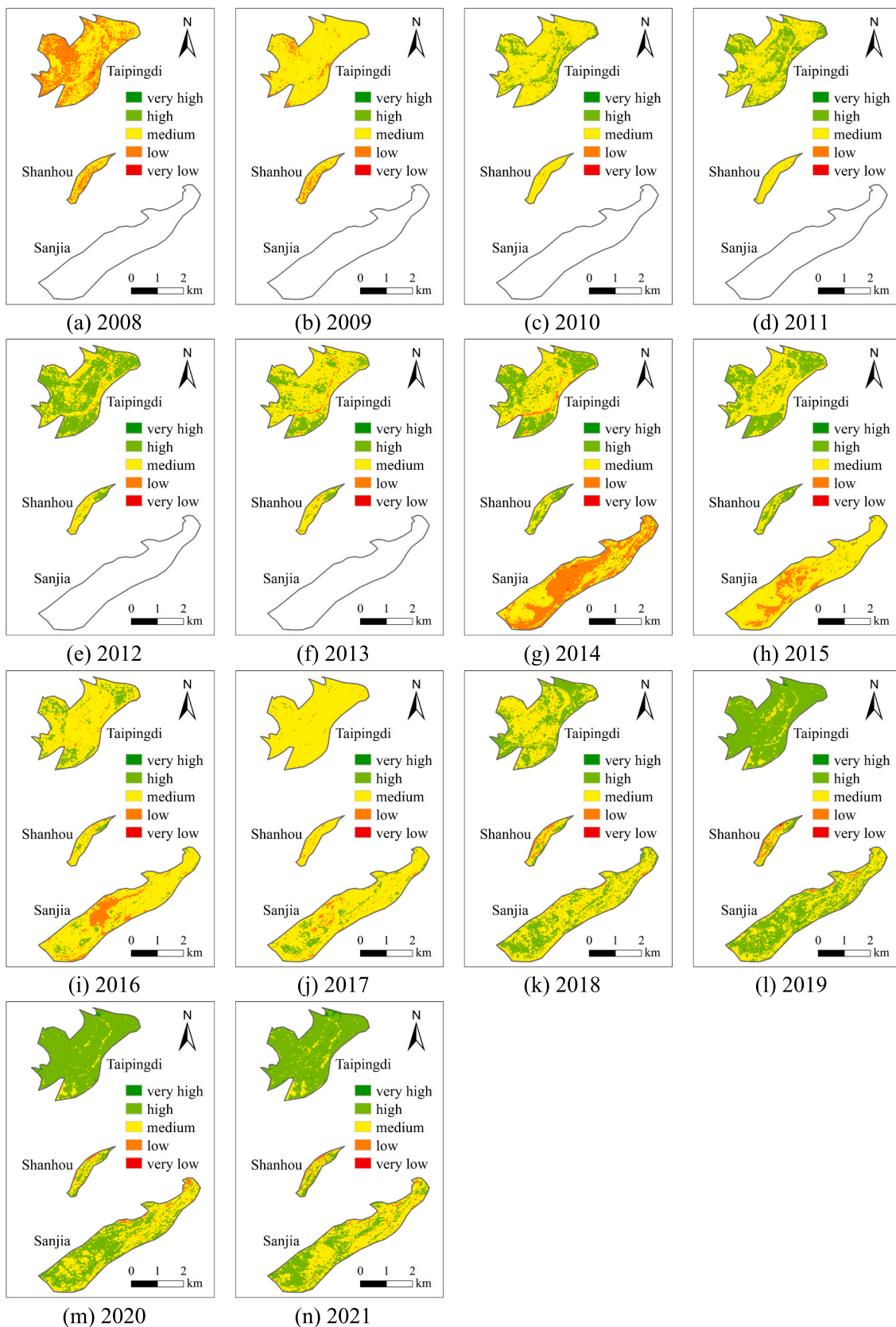


Fig. 7. Spatial distribution of classified annual maximum vegetation resilience in the dumps after restoration.

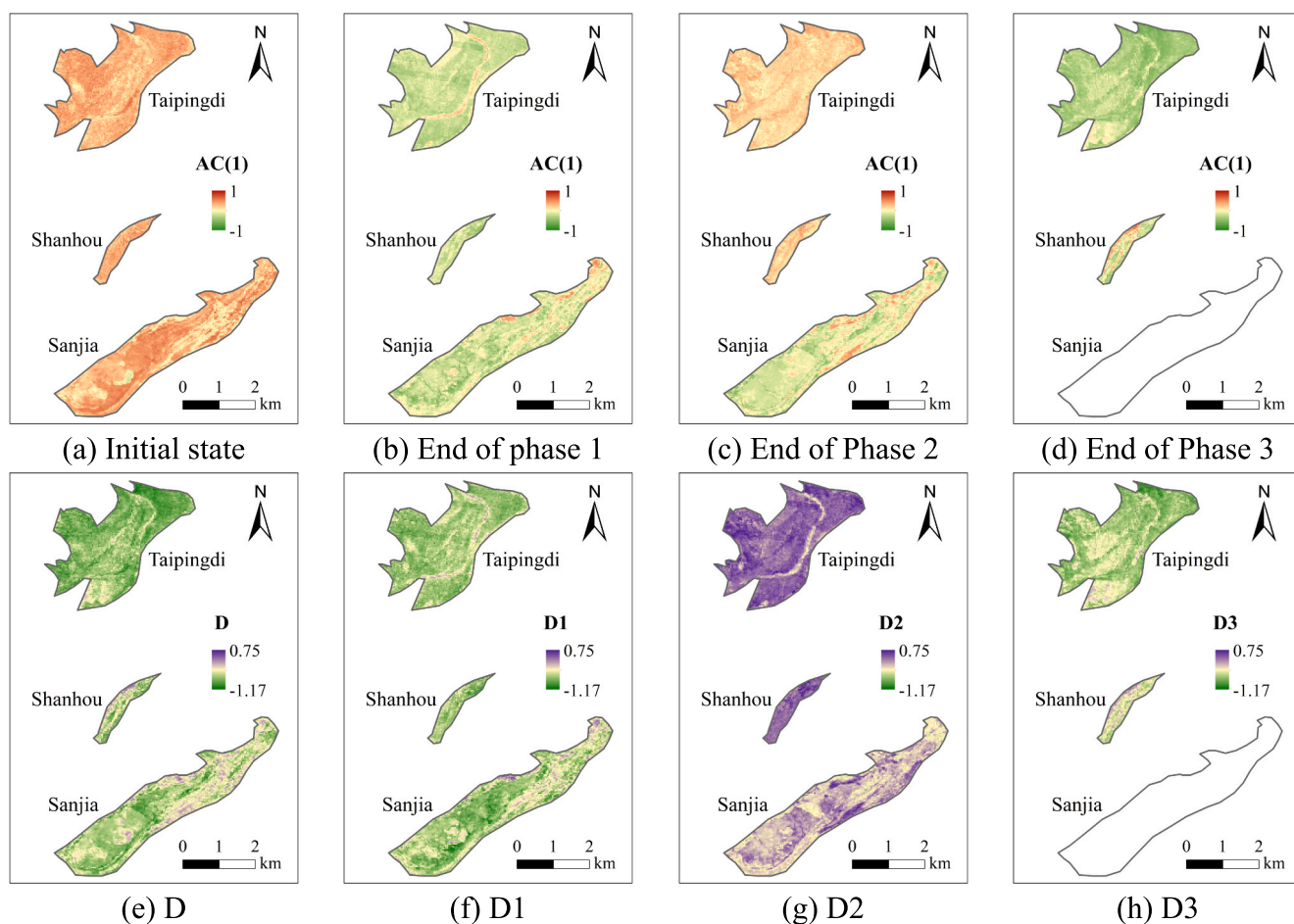


Fig. 8. Spatial distribution of vegetation resilience at initial restoration and the end of each phase, including quantitative evaluation of effectiveness.

Table 4

Proportions of areas exhibiting enhanced or declined vegetation resilience during each phase.

Phase Dump	Initial to End		Phase1		Phase2		Phase3	
	<0	>0	<0	>0	<0	>0	<0	>0
Taipingdi	99.85 %	0.15 %	98.65 %	1.36 %	2.83 %	97.17 %	99.26 %	0.75 %
Shanhou	88.58 %	11.42 %	99.69 %	0.21 %	0.62 %	99.38 %	83.74 %	16.26 %
Sanjia	94.04 %	5.96 %	95.02 %	4.98 %	44.27 %	55.73 %	—	—

resilience. These findings provide crucial insights for optimizing vegetation restoration strategies and supporting targeted measures to enhance ecological benefits at different phases of restoration.

At Taipingsdi, precipitation was the most influential climatic driver across all three phases, according to the median contributions, followed by temperature and net solar radiation. In the first phase, precipitation alone and its combined effect with temperature were the main drivers of vegetation resilience changes. Region A in the ternary diagram showed high point density, indicating a strong impact of these two climatic drivers, covering 37.82 % and 52.54 % of the area. The effect of precipitation alone was mainly concentrated around the dump’s edges, while the combined effect of precipitation and temperature was distributed in the central area. In the second phase, Region B shifted towards precipitation and net solar radiation, increasing their respective contributions. Areas driven by precipitation alone accounted for 68.82 % of the area. The influence of net solar radiation increased in the northeastern part of the dump, with the dominant type being a combination of precipitation and solar radiation, covering 11.9 % of the area. In the third phase, the number of pixels influenced solely by precipitation increased again, with an area coverage of 78.01 %. The area

affected solely by net solar radiation also increased slightly, mainly around the dirt roads and surrounding dump areas.

At Shanhou, precipitation contributed most significantly across the three phases, as indicated by median contributions, followed by net solar radiation and temperature. The dominant climatic driver types were precipitation alone and net solar radiation alone. In the first phase, the area influenced by precipitation alone accounted for 30.35 %. In comparison, net solar radiation alone accounted for 30.56 %, and the combined influence of the two covered 28.6 %, with a scattered distribution across the dump. In the second phase, the cluster shifted towards precipitation, and the area influenced by precipitation alone increased to 45.27 %, mainly distributed along the two dirt roads in the central and western parts of the dump. In the third phase, the points in the ternary diagram were more evenly distributed, with an increase in the influence of temperature. However, precipitation and net solar radiation remained the dominant drivers.

At Sanjia, during the two phases, the median contributions of climatic drivers showed that net solar radiation had the highest contribution, followed by precipitation, with temperature having the least influence. Net solar radiation alone was the primary dominant climatic

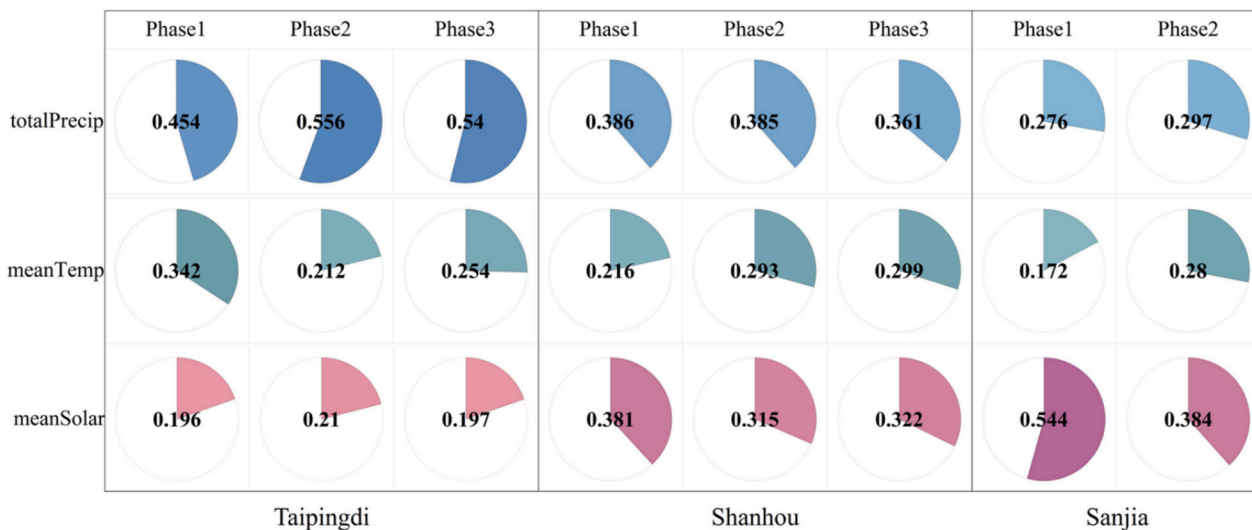


Fig. 9. Median contributions of key climatic drivers to vegetation resilience in each phase at the dumps.

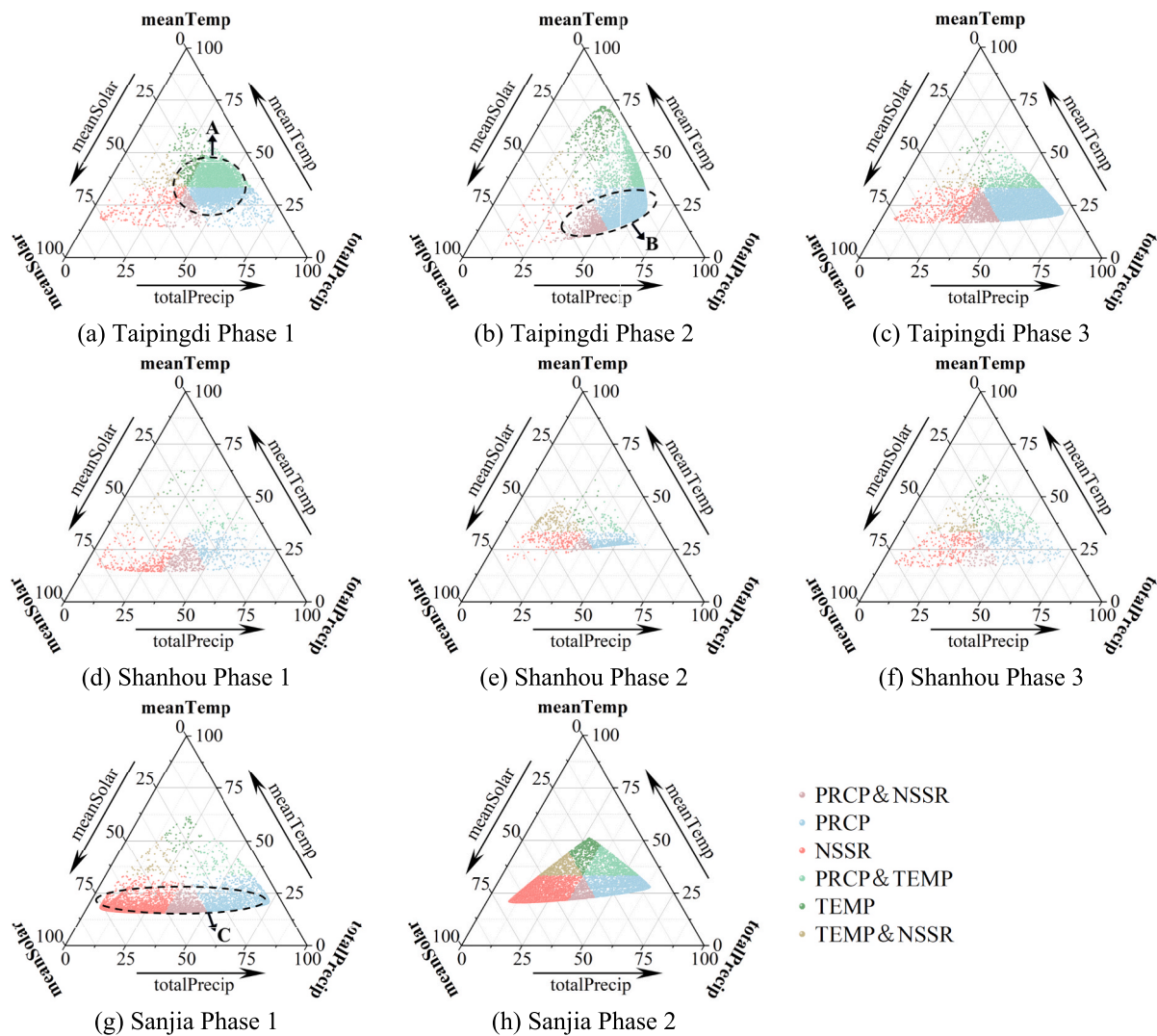


Fig. 10. Ternary diagrams of key climatic driver contributions for each phase in the dumps.

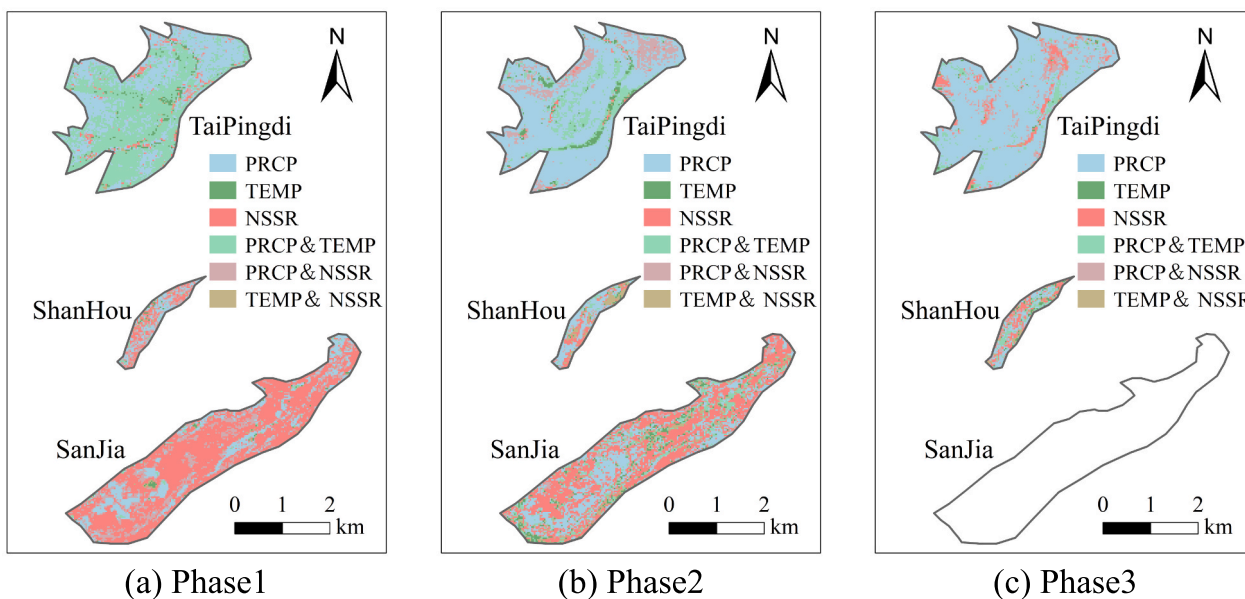


Fig. 11. Spatial distribution of dominant climatic drivers influencing vegetation resilience in each phase.

Table 5
Proportions of areas influenced by six types of dominant climatic drivers after restoration.

Dominant Drivers		PRCP	TEMP	NSSR	PRCP & TEMP	PRCP & NSSR	TEMP & NSSR
Taipingdi	Phase1	37.82 %	2.85 %	3.17 %	52.54 %	2.47 %	1.14 %
	Phase2	68.82 %	4.06 %	1.18 %	13.60 %	11.90 %	0.44 %
	Phase3	78.01 %	0.81 %	5.37 %	6.45 %	8.68 %	0.69 %
Shanhou	Phase1	30.35 %	2.26 %	30.56 %	5.45 %	28.60 %	2.78 %
	Phase2	45.27 %	2.98 %	20.06 %	6.89 %	7.61 %	17.18 %
	Phase3	29.42 %	7.41 %	26.34 %	16.05 %	11.21 %	9.57 %
Sanjia	Phase1	16.51 %	0.80 %	60.88 %	1.38 %	19.49 %	0.94 %
	Phase2	25.99 %	5.90 %	43.80 %	11.33 %	6.54 %	6.44 %

driver. In the first phase, the points in the ternary diagram clustered at Region C, indicating a low contribution from temperature. Net solar radiation alone accounted for 60.88 % of the area, covering most of the dump except for the central dirt road and the southwest mound. The two types of combined drivers involving net solar radiation and precipitation accounted for 80.37 % of the area. In the second phase, Although the dominant drivers remained unchanged, the pixel distribution became more uniform, with sporadic temperature occurrences acting as the sole driver in certain areas.

5. Discussion

5.1. Staged analysis of vegetation resilience in dumps

Vegetation resilience describes the capacity of vegetation ecosystems to recover to a sustainable state following environmental disturbances, crucial for ecosystem adaptation and long-term sustainability (Elmqvist et al., 2003). To verify the reliability of the vegetation resilience results, we calculated the first-order autocorrelation coefficient AC(1) using sliding windows of 3, 4, 5, and 6 years, with experimental results showing similar fluctuations across different window sizes. Comparing vegetation resilience curves obtained with different sliding windows and the restoration timelines of the three dumps, we determined that a 4-year window was optimal.

Integrating CSD theory with remote sensing technology provides novel insights into vegetation ecosystems stability across different restoration phases in mining environments. CSD theory effectively captures “critical transitions,” while remote sensing delivers high-resolution data for monitoring restoration. Based on this, we observed

an interesting phenomenon at Pingzhuang West Opencast Coal Mine dumps: vegetation resilience experienced three phases—significant enhancement, decline, and renewed enhancement. During the first phase, introducing restoration measures led to rapid vegetation growth, indicating strong self-repair and adaptive capacity. However, these responses were mainly driven by external interventions rather than spontaneous ecosystem regulation. In the second phase, the vegetation entered a ‘bottleneck’ period, with slowed growth likely resulting from nutrient depletion and increased competition. This resource limitation diminished resilience, a common issue in mine restoration that frequently results in stagnation or delayed recovery (Meuser, 2012; Morel et al., 2015). In the third phase, vegetation ecosystem gradually recovers through self-regulation, stabilizing with optimized plant structures and strengthened root networks, enhancing resilience and allowing it to cope better with external disturbances. This three-phase model illustrates a typical transition trajectory from external dependency to self-regulation, highlighting different ecological mechanisms and their responses to disturbances at each phase (Tittonell, 2020).

However, NDVI fails to capture this phenomenon because it mainly reflects the current greenness of vegetation. AC(1) reflects different information by emphasizing vegetation self-repair and adaptability. To enable a direct comparison of the staged characteristics between NDVI and AC(1), we extracted both indicators using the same sliding window approach, thereby minimizing seasonal interference. Results shown in Fig. 12 indicate that AC(1) captures aspects of vegetation resilience that NDVI cannot detect, particularly in revealing the internal dynamics of ecosystem resilience across the three phases. This stage characteristic is consistent with the research results of Gillson et al. (Gillson and Ekblom,

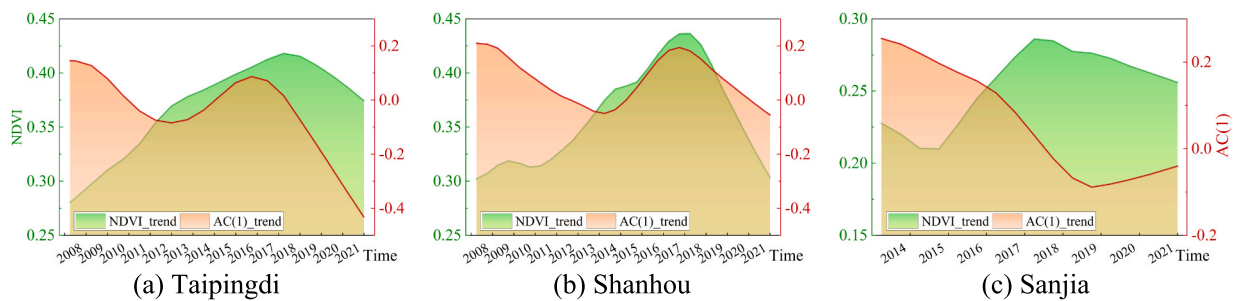


Fig. 12. Comparison of NDVI and AC(1) trends in each dump.

2009; Shilpakar et al., 2021; Kusch et al., 2022). The finding provides data support for the quantitative assessment of vegetation resilience at different stages. Additionally, we found that vegetation resilience does not always increase concurrently with greening. This finding aligns with Wang et al.'s research on the Loess Plateau of China (Wang et al., 2023 (b)). These observations suggest that relying solely on NDVI may not fully capture the restoration process of vegetation ecosystems. Identifying and analyzing the staged characteristics of vegetation resilience can help strengthen monitoring and management during critical periods, thereby achieving sustainable ecosystem recovery.

5.2. Climatic influences of vegetation resilience in dumps

Previous studies, including those by Isbell et al., 2015, have demonstrated the significant influence of key climatic drivers such as precipitation, temperature, and net solar radiation on vegetation resilience (Isbell et al., 2015; Hossain et al., 2023; Luo et al., 2024). Our study found that the main climatic drivers of vegetation resilience varied among the dumps. At Taipingdi, precipitation contributed most significantly to vegetation resilience. At Shanhou, both precipitation and net solar radiation were important contributors. Moreover, at Sanjia, net solar radiation was the dominant driver. Field investigations and literature analysis revealed that Taipingdi's vegetation primarily consists of species like *Populus simonii* and sea buckthorn. The shallow roots of *Populus simonii* make it highly dependent on surface soil moisture (Zhai et al., 2023), and the loose soil and weak water retention capacity in the area limit water uptake from deeper soil, making vegetation heavily reliant on precipitation. The restoration efforts at Shanhou were less intensive, resulting in a balanced soil structure that retains some moisture while providing good aeration. This balance supports water retention and sunlight penetration, making precipitation and net solar radiation significant contributors to vegetation resilience. Sanjia's vegetation mainly consists of pine, a drought-tolerant, deep-rooted species (Ne'eman and Osem, 2021) capable of accessing groundwater. The hard soil in the area also retains moisture well, reducing the vegetation's reliance on surface water and making net solar radiation a more critical driver for photosynthesis. Additionally, the influence of climatic drivers on vegetation resilience was consistent across different phases, indicating that the underlying conditions, such as soil texture and vegetation type, partly determined the vegetation's sensitivity to climatic drivers. Therefore, the Pingzhuang West Opencast Coal Mine's Taipingdi dump and Houshan dump could be properly irrigated for future management, and a mixture of trees could also be planted for all dumps to enhance and stabilize vegetation resilience. This approach can improve long-term ecosystem stability while reducing future restoration and maintenance costs, thereby offering both ecological and economic benefits.

5.3. Limitations and future work

This study employed the concept of vegetation resilience, which has potential and limitations (Dakos et al., 2015; Liu et al., 2019). The

metric, as measured by AC(1), is grounded in CSD theory, which allows for the estimation of recovery capacity without controlled experiments (Smith et al., 2022). This approach primarily relies on long-term satellite vegetation index datasets (Zeng et al., 2022). Previous studies have demonstrated its effectiveness by comparing the metric with empirically estimated recovery rates following disturbances (Smith and Boers, 2022; Smith et al., 2023). However, the resilience signal provided by CSD theory mainly serves as an early warning rather than a definitive prediction of critical ecological shifts (Kéfi et al., 2013).

To enhance the practical applicability and policy relevance of the findings, we propose two key areas for future research: First, efforts should be directed toward establishing clearer connections between vegetation resilience metrics and actual critical transitions in mining ecosystems (Forzieri et al., 2022). Second, comparative studies across opencast mining regions in neighboring provinces, as well as across different climatic zones, are needed to better understand how restoration outcomes vary under diverse environmental conditions. Such studies would contribute to distinguishing generalizable patterns from region-specific resilience responses.

6. Conclusions

This study developed a vegetation resilience indicator based on CSD theory and long-term Landsat quantitative remote sensing, providing insights into vegetation ecosystems' self-repair and adaptive capacity in opencast coal mine dumps. Compared to traditional fixed-window approaches, the pixel-adaptive MultiRes method has a wide range of stability. Based on the resilience indicator AC(1), we conducted a comprehensive analysis to assess spatiotemporal dynamics, effects, and key climatic influences on vegetation resilience after restoration. This study addresses issues that remain unresolved in previous vegetation research on opencast coal mine dumps. We have come to the following conclusions:

(1) This study identified a phased progression in the self-repair and adaptive capacity of vegetation in the Pingzhuang West Opencast Coal Mine dumps after restoration. Vegetation resilience followed a distinct "three-phase" temporal trajectory: significant enhancement, decline, and renewed enhancement. In the first phase, resilience significantly improved, with the dominant resilience levels shifting from "low" and "medium" to "medium" and "high." During the second phase, the vegetation's capacity for self-repair and adaptation declined. Among the three dumps, Taipingdi experienced the most rapid deterioration, followed by Sanjia and Shanhou. In the third phase, both Taipingdi and Shanhou demonstrated renewed enhancement in vegetation resilience. Taipingdi exhibited predominantly "high" annual maximum resilience levels, while Shanhou displayed a comparatively gradual recovery.

(2) Following years of natural self-regulation and adaptation, vegetation resilience in the dumps significantly improved compared to the initial fragile ecosystem. Over 88 % of the area showed resilience enhancement, with Taipingdi experiencing the most notable increase, reaching 99.85 %. Over 95 % of each dump area exhibited improved resilience in the first phase. However, the second phase saw a

widespread decline, particularly in Taipingdi and Shanhou, where 97.17 % and 99.38 % of the areas experienced decreased resilience. In the third phase, 99.26 % of Taipingdi and 83.74 % of Shanhou experienced resilience enhancement, though the magnitude of improvement was smaller compared to the first phase.

(3) Vegetation resilience sensitivity to climatic drivers remained relatively stable over time, particularly during the first and third phases. Key climatic drivers, including precipitation, temperature, and net solar radiation, played key roles in vegetation resilience dynamics. While the contribution ranking of these drivers differed across the dumps, it remained consistent within each dump throughout all phases. At Taipingdi, precipitation contributed the most, followed by temperature and net solar radiation. At Shanhou, precipitation and net solar radiation were the most significant contributors, followed by temperature. At Sanjia, net solar radiation was the primary driver, followed by precipitation and temperature. Moreover, areas dominated by a single climatic driver were generally more significant than those dominated by a combination of two drivers, with precipitation and net solar radiation playing significant roles in vegetation resilience dynamics.

CRediT authorship contribution statement

Hui Wang: Writing – original draft, Visualization, Methodology, Formal analysis, Conceptualization. **Chengye Zhang:** Writing – review & editing, Project administration, Methodology, Funding acquisition. **Yaxin Ding:** Visualization, Investigation. **Feiyue Li:** Visualization, Investigation. **Wanxi Liu:** Visualization, Investigation. **Yan Ma:** Visualization, Investigation, Funding acquisition. **Yingjie Guo:** Writing – review & editing, Resources, Data curation. **Bikram Banerjee:** Writing – review & editing, Data curation. **Jun Li:** Writing – review & editing, Writing – original draft, Visualization, Methodology, Funding acquisition.

Declaration of competing interest

The authors declare that they have no known competing financial interests or personal relationships that could have appeared to influence the work reported in this paper.

Acknowledgements

This work was supported by the National Natural Science Foundation of China (42371347), the Fundamental Research Funds for the Central Universities (2022JCCXDC04), and the Open Fund of the Laboratory for Earth Surface Processes, Ministry of Education, Peking University.

Disclosure statement.

No potential conflict of interest was reported by the authors.

Code availability.

The GEE codes used to produce the seasonal maximum NDVI dataset is available to the public at

<https://code.earthengine.google.com/596b1448da7635b6ee160a8e54425fdc?noload=true>

Appendix A. Supplementary data

Supplementary data to this article can be found online at <https://doi.org/10.1016/j.jag.2025.104646>.

Data availability

The GEE codes used to produce the seasonal maximum NDVI dataset is available to the public at <https://code.earthengine.google.com/596b1448da7635b6ee160a8e54425fdc?noload=true>

References

- Antwi, E., et al., 2008. Detecting the effect of disturbance on habitat diversity and land cover change in a post-mining area using GIS. *Landsc. Urban Plan.* 87 (1), 22–32.
- Apaydin, H., et al., 2021. Artificial intelligence modelling integrated with Singular spectral analysis and seasonal-trend decomposition using loess approaches for streamflow predictions. *J. Hydrol.* 600, 126506.
- Boulton, C.A., et al., 2022. Pronounced loss of Amazon rainforest resilience since the early 2000s. *Nat. Clim. Chang.* 12 (3), 271–278.
- Dakos, V., et al., 2012. Methods for detecting early warnings of critical transitions in time series illustrated using simulated ecological data. *PLoS One.* 7 (7), e41010.
- Dakos, V., et al., 2015. Resilience indicators: prospects and limitations for early warnings of regime shifts. *Philos. Trans. r. Soc. Lond., b, Biol. Sci.* 370 (1659), 20130263.
- Dakos, V., et al., 2010. Spatial correlation as leading indicator of catastrophic shifts. *Theor. Ecol.* 3, 163–174.
- Diks, C., et al., 2019. Critical slowing down as an early warning signal for financial crises? *Empir. Econ.* 57, 1201–1228.
- Elmqvist, T., et al., 2003. Response diversity, ecosystem change, and resilience. *Front. Ecol. Environ.* 1 (9), 488–494.
- Flores, B., et al., 2024. Critical transitions in the Amazon forest system. *Nature.* 626, 555–564.
- Forzieri, G., et al., 2022. Emerging signals of declining forest resilience under climate change. *Nature.* 608 (7923), 534–539.
- Ghalehtemouri, K., et al., 2024(a). Flood risk assessment through rapid urbanization LULC change with destruction of urban green infrastructures based on NASA landsat time series data: a case of study Kuala Lumpur between 1990–2021. *ecological. Frontiers.* 44 (2), 289–306.
- Ghalehtemouri, K., et al., 2024(b). Spatial and temporal water pattern change detection through the normalized difference water index (NDWI) for initial flood assessment: a case study of Kuala Lumpur. *J. Adv. Res. Fluid Mech. Therm. Sci.* 114 (1), 178–187. *Lumpur 1990 and 2021.*
- Gillson, L., Ekblom, A., 2009. Resilience and thresholds in savannas: nitrogen and fire as drivers and responders of vegetation transition. *Ecosystems* 12, 1189–1203.
- Golestani, Z., et al., 2024. Impact of urban expansion on the formation of urban heat islands in Isfahan, Iran: a satellite base analysis (1990–2019). *J. Geovisual. Spatial Anal.* 8 (2), 32.
- Grömping, U., 2007. Relative importance for linear regression in R: the package relaimpo. *J. Stat. Softw.* 17, 1–27.
- Hancock, G., et al., 2020. Mining rehabilitation—using geomorphology to engineer ecologically sustainable landscapes for highly disturbed lands. *Ecol. Eng.* 155, 105836.
- Hossain, M., et al., 2023. Long-term evidence of differential resistance and resilience of grassland ecosystems to extreme climate events. *Environ. Monit. Assess.* 195 (6), 734.
- Hu, M., Xia, B., 2019. A significant increase in the normalized difference vegetation index during the rapid economic development in the Pearl River Delta of China. *Land Degrad. Dev.* 30 (4), 359–370.
- Huang, S., et al., 2021. A commentary review on the use of normalized difference vegetation index (NDVI) in the era of popular remote sensing. *J. For.* 32 (1), 1–6.
- Hutayanon, T., Somprasong, K., 2023. Application of integrated spatial analysis and NDVI for tree monitoring in reclamation area of coal mine. *Environ. Sci. Pollut.* 1–11.
- Imani, S., Keogh, E., 2021. Multi-window-finder: domain agnostic window size for time series data. *Proceedings of the MileTS 21*, 1–12.
- Isbell, F., et al., 2015. Biodiversity increases the resistance of ecosystem productivity to climate extremes. *Nature.* 526 (7574), 574–577.
- Kamran, J., et al., 2024. Application of Cellular automata and Markov chain model for urban green infrastructure in Kuala Lumpur. *Malaysia. Reg. Sustain.* 5 (4), 100179.
- Kéfi, S., et al., 2013. Early warning signals also precede non-catastrophic transitions. *Oikos.* 122 (5), 641–648.
- Kendall, M.G., 1938. A new measure of rank correlation. *Biometrika.* 30 (1–2), 81–93.
- Kusch, E., et al., 2022. Vegetation-memory effects and their association with vegetation resilience in global drylands. *J. Ecol.* 110 (7), 1561–1574.
- Li, J., et al., 2015. Reconstructing disturbance history for an intensively mined region by time-series analysis of landsat imagery. *Environ. Monit. Assess.* 187, 1–17.
- Li, H., et al., 2021. Regional contributions to interannual variability of net primary production and climatic attributions. *Agric. for Meteorol.* 303, 108384.
- Li, J., et al., 2024(a). Automated generation of consistent annual maximum NDVI on coal bases with a new algorithm. *Scientific Data.* 11, 689.
- Li, J., et al., 2024(b). Analysis of vegetation restoration effect and attribution of pingzhuang west open pit mine based on landsat remote sensing images. *Green Mines.* 2 (1), 31–40.
- Liu, Y., et al., 2019. Reduced resilience as an early warning signal of forest mortality. *Nat. Clim. Chang.* 9, 880–885.
- Liu, Y., et al., 2024. Vegetation resilience assessment and its climatic driving factors: evidence from surface coal mines in northern China. *Sci. Total Environ.* 945, 173803.
- Luo, M., et al., 2024. Global vegetation productivity has become less sensitive to drought in the first two decades of the 21st century. *Int. J. Appl. Earth Obs. Geoinf.* p. 135.
- McDougall, A., et al., 2013. Diversity loss with persistent human disturbance increases vulnerability to ecosystem collapse. *Nature* 494, 86–89.
- Meisel, C., et al., 2015. Critical slowing down governs the transition to neuron spiking. *PLoS Comput. Biol.* 11 (2), e1004097.
- Meuser, H. *Soil remediation and rehabilitation: treatment of contaminated and disturbed land.* Vol. 23. Springer Science & Business Media, 2012.

- Morel, J., et al., 2015. Ecosystem services provided by soils of urban, industrial, traffic, mining, and military areas (SUITMAS). *J. Soils Sediments*. 15, 1659–1666.
- Muñoz Sabater, J., 2021. ERA5-land hourly data from 1981 to present. Copernicus Climate Change Service (C3S) Climate Data Store (CDS).
- Nasr, T., et al., 2025. Predicting urban green infrastructures of ecosystem Services in Tehran Metropolitan Area Sprawl with landsat satellite time series data. *J. Archit. Plan. Res. Stud.* 22 (1), 268554.
- Ne'eman, G., Osem, Y., 2021. Pines and their mixed Forest ecosystems in the Mediterranean Basin. Springer International Publishing.
- Scheffer, M., et al., 2009. Early-warning signals for critical transitions. *Nature*. 461 (7260), 53–59.
- Scheffer, M., et al., 2015. Generic indicators of ecological resilience: inferring the chance of a critical transition. *Annu. Rev. Ecol. Evol. Syst.* 46, 145–167.
- Seddon, A., et al., 2016. Sensitivity of global terrestrial ecosystems to climate variability. *Nature*. 531 (7593), 229–232.
- Shiekh, R., El-Hashash, E., 2022. A comparison of the Pearson, Spearman rank and kendall tau correlation coefficients using quantitative variables. *Asian J. Probab. Stat.* 36–48.
- Shilpakar, R., et al., 2021. The resilience of a floodplain vegetation landscape. *Landsc. Ecol.* 36, 139–157.
- Smith, T., Boers, N., 2022. Empirical evidence for recent global shifts in vegetation resilience. *Nat. Clim. Chang.* 12 (5), 477–484.
- Smith, T., et al., 2023. Global vegetation resilience linked to water availability and variability. *Nat. Commun.* 14 (1), 498.
- Tittonell, P., 2020. Assessing resilience and adaptability in agroecological transitions. *Agric. Syst.* 184, 102862.
- Van Belzen, J., et al., 2017. Vegetation recovery in tidal marshes reveals critical slowing down under increased inundation. *Nat. Commun.* 8, 15811.
- Van Greunen, J., et al., 2014. The prominence of stationarity in time series forecasting. *Stud. Econ. Econometr.* 38 (1), 1–16.
- Van Meerbeek, K., et al., 2021. Unifying the concepts of stability and resilience in ecology. *J. Ecol.* 109 (9), 3114–3132.
- Wang, R., et al., 2012. Flickering gives early warning signals of a critical transition to a eutrophic lake state. *Nature*. 492 (7429), 419–422.
- Wang, Z., et al., 2020. Mapping the cumulative impacts of long-term mining disturbance and progressive rehabilitation on ecosystem services. *Sci. Total Environ.* 717, 137214.
- Wang, S., et al., 2023(a). Drylands contribute disproportionately to observed global productivity increases. *Sci. Bull.* 68 (2), 224–232.
- Wang, Z., et al., 2023(b). Vegetation resilience does not increase consistently with greening in China's loess Plateau. *Commun. Earth Environ.* 4 (1), 336.
- Wichers, M., et al., 2016. Critical slowing down as a personalized early warning signal for depression. *Psychother. Psychosom.* 85 (2), 114–116.
- Worlanyo, A., Jiangfeng, L., 2021. Evaluating the environmental and economic impact of mining for post-mined land restoration and land-use: a review. *J. Environ. Manage.* 279, 111623.
- Xu, W., et al., 2013. Comparison of Spearman's rho and kendall's tau in normal and contaminated normal models. *IEEE Trans. Signal Process.* 93 (1), 261–276.
- Yang, S., et al., 2022. Spatiotemporal variations of water productivity for cropland and driving factors over China during 2001–2015. *Agric. Water Manag.* 262, 107328.
- Yao, Y., et al., 2018. Spatiotemporal pattern of gross primary productivity and its covariation with climate in China over the last thirty years. *Glob. Chang. Biol.* 24 (1), 184–196.
- Zeng, Y., et al., 2022. Optical vegetation indices for monitoring terrestrial ecosystems globally. *Nat. Rev. Earth Environ.* 3 (7), 477–493.
- Zhai, Q., et al., 2023. Transpiration water consumption by *Salix matsudana* and *Populus simonii* and water use patterns at different developmental stages on sandy land. *Water*. 15 (24), 4255.
- Zhang, C., et al., 2023. Assessing the effect, attribution, and potential of vegetation restoration in open-pit coal mines' dumping sites during 2003–2020 utilizing remote sensing. *Ecol. Indic.* 155, 111003.
- Zhang, M., et al., 2019. Tempo-spatial changes and main anthropogenic influence factors of vegetation fractional coverage in a large-scale opencast coal mine area from 1992 to 2015. *J. Clean. Prod.* 232, 940–952.